Application of On-Wafer TRL Calibration on the Measurement of Microwave Properties of $Ba_{0.5}Sr_{0.5}TiO_3$ Thin Films

Hang-Ting Lue and Tseung-Yuen Tseng, *Senior Member, IEEE*

***Abstract*—A series of Al/$Ba_{0.5}Sr_{0.5}TiO_3$(BST)/sapphire multi-layered coplanar waveguide (CPW) transmission lines of different geometries and thin-film configurations was fabricated. We employed an accurate on-wafer Through-Line-Reflect (TRL) calibration technique and quasi-TEM analysis to measure the dielectric constant, loss tangent, and tunability of BST thin films using this CPW structure. Experimental results show that the overall insertion loss is less than 3 dB/cm even at frequencies as high as 20 GHz, which is the lowest obtained to date for metal/BST CPW devices. This result indicates that, with optimized impedance matching, normal conductors are also possibly suitable for fabricating low-loss tunable phase-shifter devices.**

I. Introduction

Electrically tunable nonlinear ferroelectric micro- past few years for their great potential in the application of tunable phase shifters [1]–[3], filters [4], and resonators [5]. The dielectric constant of ferroelectric materials can be controlled electrically by the applied DC bias. Compared with the conventional magnetic-controlled ferromagnetic devices and PIN diode phase shifters, they have the advantages of low cost, small size, and convenience for tuning. However, experiments have found that these devices exhibit rather high loss. For reduction of loss, the integration of superconductors with ferroelectric thin films such as $SrTiO_3$ (STO) and BST is considered to be a suitable candidate, because superconductors are extremely low-loss and the multilayered structures of $YBa_2Cu_3O_9$/STO (or BST)/$LaAlO_3$ are all compatible in the thin film process. That is, high quality thin films can be deposited in these multi-layered structures. However, the incorporation of superconductors will inevitably limit the commercial application of ferroelectric devices because additional cooling systems are needed. Additionally, for the deposition of high quality superconductors, expensive substrates such as $LaAlO_3$ are used, increasing the total cost of the devices. Hence, as these facts indicate, microwave ferroelectric devices still have quite limited applications. We have examined several previous works [2], [3], [11]–[13] carefully and found that the dominant insertion loss of most ferroelectric devices was not because of the conductor loss or the dielectric loss but instead because of the impedance mismatch. Most researchers did not design a 50-Ω matching transmission line for their devices because the dielectric constant of ferroelectric thin films was not known before the measurement and only a matching transmission line without a dielectric layer could be designed. But, after the high dielectric constant thin film was deposited on the substrate, the effective dielectric constant ε_{eff} was increased, which caused the characteristic impedance to be decreased. Therefore, there is an impedance mismatch, and a large fraction of the incident microwave signal reflects at the junctions. This phenomenon results in relatively high insertion loss and low return loss in most devices. To design matching transmission lines accurately requires accurate measurement of the dielectric constant of ferroelectric thin films. Most researchers [1]–[3], [11]–[13] designed a simple transmission line, such as multi-layered CPW phase shifter. The phase shift of transmission coefficient S_{21}, $\Delta\phi_{S_{21}}$, is given by

$$\Delta\phi_{s_{21}} = -\frac{\sqrt{\varepsilon_{eff}} \cdot f \cdot 2\pi L}{c}, \tag{1}$$

where c is the velocity of light, f is the frequency, and L is the length of transmission line. From the slope of $\Delta\phi_{S_{21}}$ versus frequency, the effective dielectric constant ε_{eff} is calculated, and the dielectric constant of thin film ε_{r2} can be extracted by a closed-form formula derived by conformal mapping [6]. However, because the transmission line is mismatched, multiple reflections will occur at the junctions, and the transmission coefficient S_{21} will exhibit interference characteristics. Because of this situation, (1) is consequently invalid. In addition, tapers between much wider electrical probing pads and narrow transmission lines are usually incorporated to provide smooth transitions. These structures act as reactance in the circuits leading to the distortion of the phase response. Therefore, to measure the dielectric constant accurately, these effects should be taken into account.

In this work, we apply a new on-wafer TRL calibration to measure the dielectric constant and loss tangent of BST thin films with Al as conductors. An overall insertion loss per centimeter (or attenuation constant α) of less than 3 dB/cm at 20 GHz and a return loss of greater than 50 dB can be obtained with proper impedance matching. This

Manuscript received October 4, 2000; accepted March 20, 2001. This work was funded by the National Science Council of the Republic of China under contract number NSC-89-2212-E-009-081.

H.-T. Lue and T.-Y. Tseng are with the Department of Electronics Engineering and Institute of Electronics, National Chiao Tung University, Hsinchu, Taiwan, Republic of China (e-mail: tseng@cc.nctu.edu.tw).

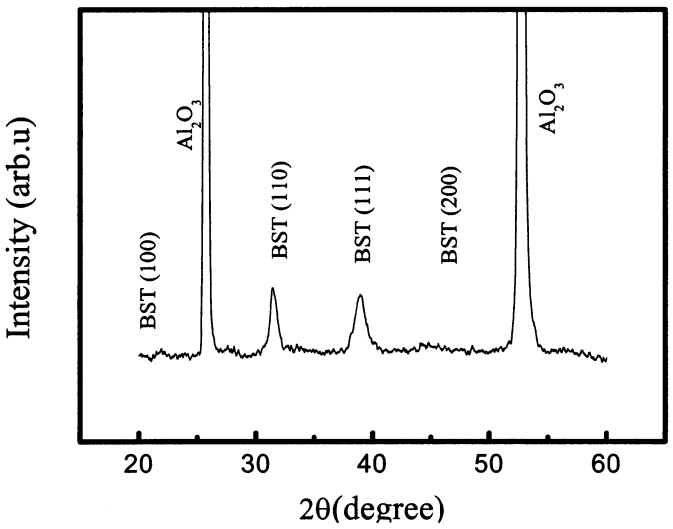

Fig. 1. X-ray diffraction pattern of BST thin film on sapphire.

result is much better than all other reported results [2], [3] with normal metal as conductors and even better than some results with superconductors. Therefore, we point out that the conductor loss of normal metals might be overestimated; if careful design of impedance matching is carried out, the insertion loss of ferroelectric devices can be remarkably reduced.

II. Samples Preparation

BST thin films were deposited on (1120) sapphire (Al_2O_3) substrate by radio-frequency magnetron sputtering. All samples were prepared at a fixed power of 100 W and a constant pressure of 40 mTorr with $Ar{:}O_2 = 9{:}1$.The substrate temperature was held at 600°C. A two-step growth technique was employed. First, a thin (10 nm) amorphous layer of BST was deposited at room temperature. The substrate temperature was then increased to 600°C and a second BST film was deposited. After deposition, some samples were annealed in O_2 atmosphere at 800°C using a rapid thermal annealing for 10 min with heating rate 80°C/s. Then, Al metal electrodes with 1-μm thickness were deposited by thermal evaporation. Finally, standard photolithography and etching were carried out to form the desired CPW transmission line patterns. The X-ray spectrum as shown in Fig. 1 clearly indicates that the BST thin films are well crystallized as deposited.

The thickness of the BST thin films range from 2400 to 5000 Å; the buffer layers (amorphous BST films) were much thinner than the total thickness. Therefore, our calculation measures the average properties of the BST thin films and neglects the buffer layers. Several samples and one bare sapphire wafer were measured as described in Table I.

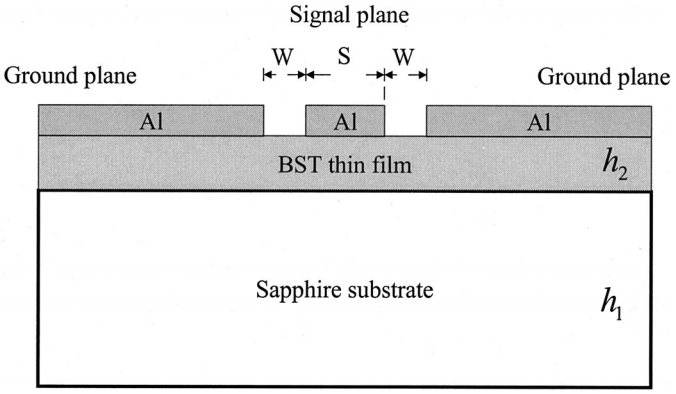

Fig. 2. Cross-section view of multi-layered CPW structure.

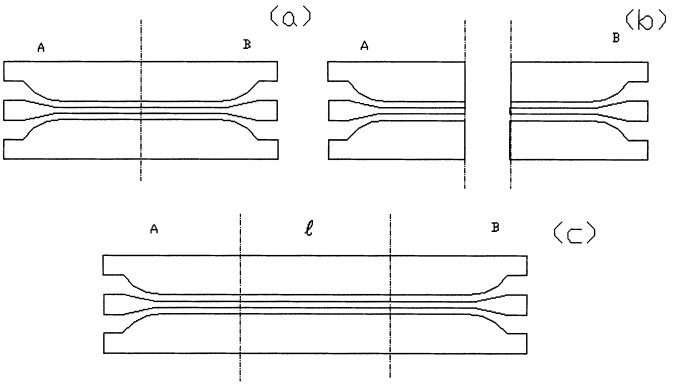

Fig. 3. Diagram of a) "Thru" with reference planes directly connected, b) "Reflect" with both reference planes opened, and c) "Line" with reference planes connected by a matching line.

III. CPW Transmission Line Design and Measurement

Using a value of $\varepsilon_{r1} \approx 10$ for the sapphire substrate and the conformal mapping formula [6], the center conductor width (S) and gap width (W) as shown in Fig. 2 are designed to be 50 and 20 μm, respectively. Substrate thickness is 500 μm, which is much larger than the linewidth. Because the electromagnetic field is confined within the gap, we can expect that the back side of the substrate has no influence on the performance of the devices. The patterns for TRL calibration, "thru," "reflect," and "line," were designed in the mask, as illustrated in Fig. 3, which shows that they have the same transition regions A and B with tapers. The tapers were designed to have gradually wider line width with an equal ratio of $S{:}W$. The final centered pad size is 150 μm, and the distance of pitch to pitch is also 150 μm for providing the contact of the coplanar probe (GSG). The total length of "thru" is 5660 μm, and the reference plane (dashed line) is away from the tapers by 2000 μm. Each "reflect" is terminated by open, and the "line" is made by connecting A and B with length of $\ell_1 = 6000$ μm or $\ell_2 = 8000$ μm. These four test kits were made on the same wafer in a 2-cm × 2-cm, one-sided polished sapphire wafer.

TABLE I
SUMMARY OF Al/BST/SAPPHIRE CPW DEVICE PARAMETERS.

Sample	Buffer layer	RTA treatment	Film thickness (Å)	q_2	ε_{eff}	ε_{r2}	$\phi_0(^\circ)$	$Z_c(\Omega)$	S/W
Bare	—	—	—	—	5.27	—	0.9	50.4	2.55
D1	No	No	2400	0.0073	6.47	176	1.2	45.4	1.85
D2	No	Yes	2400	0.0073	7.08	261	1.4	43.4	1.60
D3	Yes	No	2900	0.0088	6.59	161	1.4	45.0	1.79
D4	Yes	Yes	2900	0.0088	7.27	239	1.4	42.9	1.54
D5	Yes	No	4000	0.0121	7.93	231	1.3	41.1	1.35
D6	Yes	Yes	4500	0.0135	8.93	281	1.8	38.7	1.12
D7	No	Yes	8000	0.0237	10.37	225	1.9	35.9	0.87

The BST film used in D7 was sol-gel derived film.

The on-wafer measurements were carried out at a microwave probe station with an ACP probe and HP 8510C network analyzer at frequencies ranging from 100 MHz to 20 GHz. DC bias up to 40 V was applied on the signal plane through bias tees. Such "on-wafer" measurements do not require additional wire bonding or test fixtures; hence, many undesired parasitic effects are reduced. Moreover, we can carry out measurements of many patterns on one wafer if the films have good uniformity. Before measurement, standard full-to-port calibration was conducted before the probe tips. We then measured each standard at room temperature and calculated the TRL calibration by a program we developed.

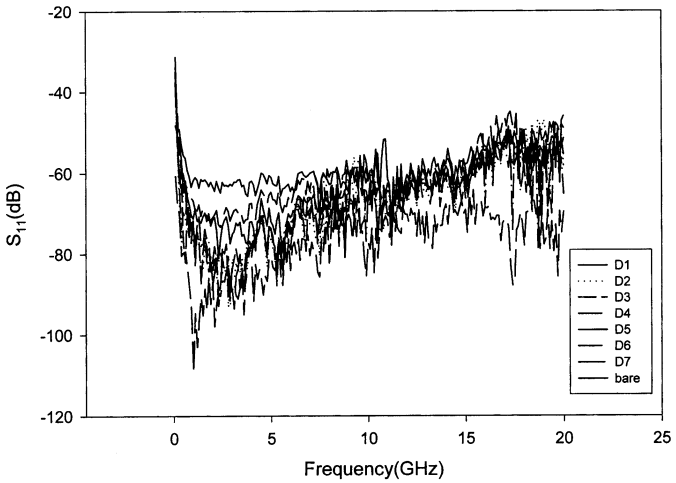

Fig. 4. De-embedded return loss S_{11} versus frequency of the CPW devices.

IV. TRL Calibration

TRL calibration is known for de-embedding the corrected response of a device under test (DUT) [7]. The purpose of TRL is to eliminate the unknown error box of transition regions A and B by calculating the "thru", "reflect," "line"; then the embedded S-matrix of the DUT can be converted to the de-embedded result, independent of A and B. The result is equivalent to moving the reference plane from the probe pad to the desired reference plane, as shown in the dashed line of Fig. 3. Because the transmission lines are identical between the two sides of the reference plane, we expect the "line" to be matched to the new reference plane. In addition, the reference plane should be far away from the discontinuous region to prevent the disturbance of local mode. It is not necessary for the "reflect" to be exactly open, but it should be identical in both two ports. The pair of "reflect" in our design are simply opened to the air. As the phase shift through ℓ is 0° or multiples of 180°, the error associated with the system becomes larger. The best accuracy is obtained at the frequency at which the length ℓ is one-quarter wavelength long or, equivalently, at a 90° phase shift. It is a common practice to limit a single line to between 20° and 160°; beyond this bandwidth, the calibration is replaced by another line. After measuring the "thru," "reflect," and "line," we can let the DUT be the "line" and calculate the de-embedded response of the line ℓ. In our devices, two different lines of length $\ell_1 = 6000$ μm and $\ell_2 = 8000$ μm were designed. The calibration was carried out by ℓ_1 at frequencies where the phase shift of ℓ_1 was changed from 0° to 160°, 200° to 340°, and 380° to 520°. Beyond these points, the calibration was replaced by ℓ_2. This test procedure is called split-band TRL calibration. After TRL calibration, the transmission line is non-reflective and matched to the new reference plane, and the effective dielectric constant and characteristic impedance can then be correctly extracted. The TRL algorithm was reported in [8], and we have made a program to calculate this calibration.

V. Extraction of Propagation Constant and Effective Dielectric Constant

We have measured several CPW devices with different geometries and configurations and one bare sapphire wafer without BST thin films. The results are listed in Table I. The TRL calibration as described previously was performed for each sample, and the de-embedded S-parameters were obtained. We can see in Fig. 4 that the return loss was larger than 50 dB, which clearly indicates

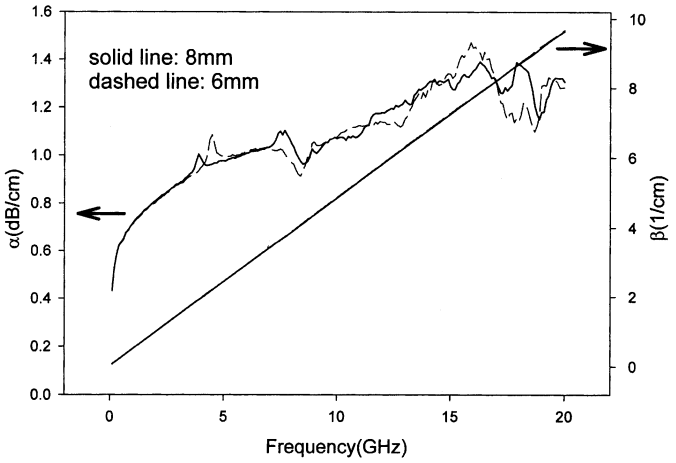

Fig. 5. Comparison of the calculated complex propagation constant for different lengths of transmission lines.

good impedance matching without reflection. Because the transmission lines of the samples are non-reflecting, the de-embedded transmission coefficient S_{21} can be directly related to the propagation constant by

$$\alpha = -\frac{S_{21}(dB)}{\ell(cm)}, \tag{2}$$

$$\beta = -\frac{\Delta\phi_{S_{21}}(\text{rad})}{\ell(cm)}, \tag{3}$$

where α is the attenuation constant (dB/cm) and β is the propagation constant (cm^{-1}). Next, we can check the consistency of the TRL calibration by comparing the de-embedded result of two different lengths ℓ_1 and ℓ_2, as shown in Fig. 5. We find that β_1 and β_2 nearly coincide with each other, and the attenuation constants α_1 and α_2 also match each other quite well. As shown in Fig. 6, straight-line curves are obtained for each sample, and the effective dielectric constant ε_{eff} can be obtained by (1). However, we found experimentally that there existed a small offset value for the phase shift $\Delta\phi_0$ at zero frequency. Therefore, we modified (1) to

$$\Delta\phi_{S_{21}} = -\frac{2\pi\sqrt{\varepsilon_{eff}}\cdot f\cdot\ell}{c} - \Delta\phi_0. \tag{4}$$

$\Delta\phi_0$ and ε_{eff} are obtained by simple straight-line curve fitting, and the results are given in Table I. The offset value $\Delta\phi_0$ may be due to a) the preliminary error of the full two-port calibration, which may be caused by the parasitic capacitance or inductance of standard short, open, load, thru (SOLT) test kits; b) variation of probe position, because we cannot make the probe at exactly the same position with every test kit; and c) TRL calibration error near zero frequency. $\Delta\phi_0$ is around 1° and not a serious problem. Note that in (4), the effective dielectric constant can be extracted at each frequency, not necessarily by curve fitting. Because all of the curves are very straight, we believe that the effective dielectric constant is almost constant over this bandwidth. However, in general, $\varepsilon_{eff}(f)$ can be obtained at each frequency, and measuring the dielectric dispersion is possible. The straight-line characteristic also indicates that the de-embedded results are free of parasitic effects caused by the discontinuous region. The extraction of the dielectric constant ε_{r2} of ferroelectric thin films is discussed in Section VI, and loss-tangent is discussed in Section VII.

VI. Quasi-TEM Analysis

Conformal mapping is a fast tool for determining the impedance and effective dielectric constant in a microstrip circuit. The simplified formulas for the two-layer CPW structure are given here [6], [9]:

$$k_0 = \frac{S}{S+2W} \tag{5}$$

$$k_1 = \frac{\sinh(\pi S/4h_1)}{\sinh(\pi(S+2W)/4h_1)} \tag{6}$$

$$k_2 = \frac{\sinh(\pi S/4h_2)}{\sinh(\pi(S+2W)/4h_2)} \tag{7}$$

$$q_i = \frac{1}{2}\frac{K(k_i)}{K'(k_i)}\frac{K'(k_0)}{K(k_0)} \qquad i=1,2 \tag{8}$$

$$\varepsilon_{eff} = 1 + q_1(\varepsilon_{r1}-1) + q_2(\varepsilon_{r2}-\varepsilon_{r1}) \tag{9}$$

$$Z_c = \frac{30\pi}{\sqrt{\varepsilon_{re}}}\frac{K'(k_0)}{K(k_0)} \tag{10}$$

where h_1 is the substrate thickness, h_2 is the film thickness, ε_{r1} is the dielectric constant of the substrate, ε_{r2} is the dielectric constant of ferroelectric thin film, and S and W are as shown in Fig. 2, $K(x)$ is the elliptical integral of the first kind, and $K'(x) \equiv K(\sqrt{1-x^2})$. q_i is the filling factor. According to (9), the contribution of the thin film to the total effective dielectric constant is directly proportional to the q_2. In other words, the q_i-factor is a measure of the proportionality of electromagnetic energy inside each dielectric layer.

If $S, W \gg h_2$, k_2 becomes too small ($k_2 < 10^{-45}$ in our case), which leads to numerical error in calculating the elliptic function. To overcome this difficulty, we employ the asymptotic formula for the ratio of elliptic function [6]:

$$\frac{K(k)}{K'(k)} = \frac{\pi}{\ln\left[\frac{2\left(1+\sqrt{\sqrt{1-k^2}}\right)}{1-\sqrt{\sqrt{1-k^2}}}\right]} \tag{11}$$

for $0 \le k \le 0.707$, when $k_2 \to 0$;

$$\frac{K(k_2)}{K'(k_2)} = \frac{\pi}{\ln\left[\frac{2\left(1+\sqrt{\sqrt{1-k_2^2}}\right)}{1-\sqrt{\sqrt{1-k_2^2}}}\right]} \approx \frac{\pi}{\ln\left[\frac{16}{k_2^2}\right]}. \tag{12}$$

Therefore,

$$q_2 = \frac{1}{2}\frac{\pi}{\ln\left[\frac{16}{k_2^2}\right]}\frac{K'(k_0)}{K(k_0)}. \tag{13}$$

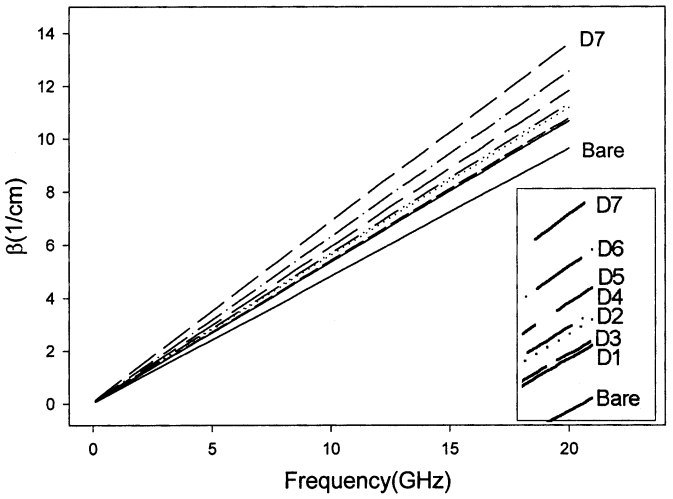

Fig. 6. Calculated propagation constant versus frequency of CPW devices.

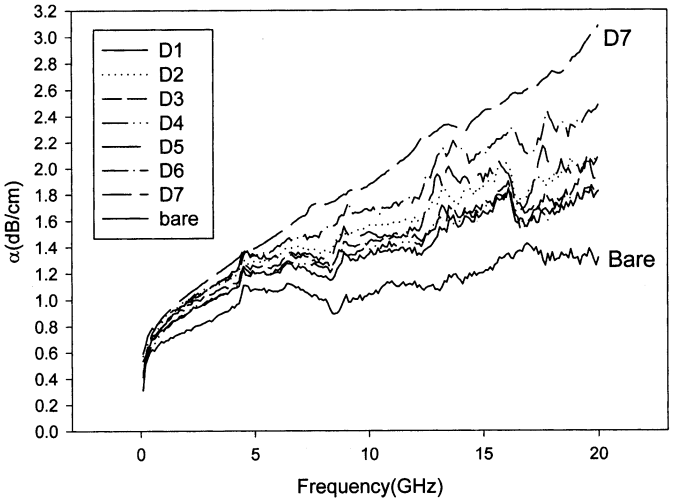

Fig. 7. The attenuation constant versus frequency of CPW devices.

Eq. (13) is analytic even at such a small k_2. Therefore, q_2 is calculated by this formula instead of (8). With substrate thickness $h_1 = 500$ μm, q_2 is calculated versus different thicknesses h_2 and different linewidths; the result is shown in Fig. 6. We find that q_2 is almost proportional to the thickness and is on the order of 1%. Therefore, a ferroelectric thin film with a dielectric constant larger than 100 is required to obtain an obvious change of the phase response. Another important feature is that the filling factor increases significantly when the linewidths decrease. This will be discussed further in Section VIII.

The effective dielectric constant of the bare sapphire wafer is 5.267, from which the dielectric constant ε_{r1} was obtained to be 9.53. Then, the dielectric constant ε_{r2} of each sample was calculated and listed in Table I.

Once the effective dielectric constant of each sample was given, the characteristic impedance Z_c of the transmission line was derived according to (10), and we can also redesign the suitable ratio of S:W with 50-Ω impedance, as listed in Table I. The accurate effective dielectric constant given by this method can provide engineers a means to design matching transmission lines to minimize the insertion loss. Another useful way to describe the transmission line is in terms of distributed resistance, inductance, conductance, and capacitance (RLGC model). These parameters are calculated by

$$j\omega C + G = \frac{\gamma}{Z_c} \quad \text{and} \tag{14}$$

$$j\omega L + R = \gamma Z_c \tag{15}$$

where $\gamma \equiv \alpha + j\beta$ is the complex propagation constant, which was directly measured as described in Section V.

Conformal mapping method is based on the quasi-TEM approximation. Because the linewidths S and W are much shorter than the electromagnetic wavelength, we expect that the quasi-TEM approximation is valid over a wide range of frequency. No rigorous analysis of a non-TEM model of CPW was reported until now; however, if the quasi-TEM approximation is broken, the effective dielectric constant $\varepsilon_{eff}(f)$ should show obvious frequency dispersion. Because this does not happen in the present study, we assume that quasi-TEM analysis is adequate in the frequency range of interest.

VII. Evaluation of Attenuation

The loss mechanisms include the conductor loss, the dielectric loss of the ferroelectric layer, the dielectric loss of substrate, and the radiation loss.

Because the sapphire is low-loss (loss tangent $< 10^{-4}$), the dielectric loss of substrate can be neglected. In addition, the line width is much shorter than the electromagnetic wavelength, so we can expect that the radiation loss can also be neglected. Therefore, we assume the loss of our devices is mainly due to conductor loss and dielectric loss of the ferroelectric layer.

For a bare sapphire wafer, the attenuation caused by conductor loss is given by [6], [10]:

$$\alpha_c = 8.68 \frac{R_s b^2}{16 Z_0 K^2(k)(b^2 - a^2)} \left(\frac{1}{a} \ln \left(\frac{2a}{\Delta} \frac{b-a}{b+a} \right) + \frac{1}{b} \ln \left(\frac{2b}{\Delta} \frac{b-a}{b+a} \right) \right) (dB/m), \tag{16}$$

in which a, b, and Δ are defined by

$$a = \frac{S}{2}, \tag{17}$$

$$b = \frac{S + 2W}{2}, \text{ and} \tag{18}$$

$$\Delta = \frac{t}{4\pi e^{\pi}} \tag{19}$$

where R_s is the surface resistance of the metal, Z_0 is the characteristic impedance, and t is the metal thickness.

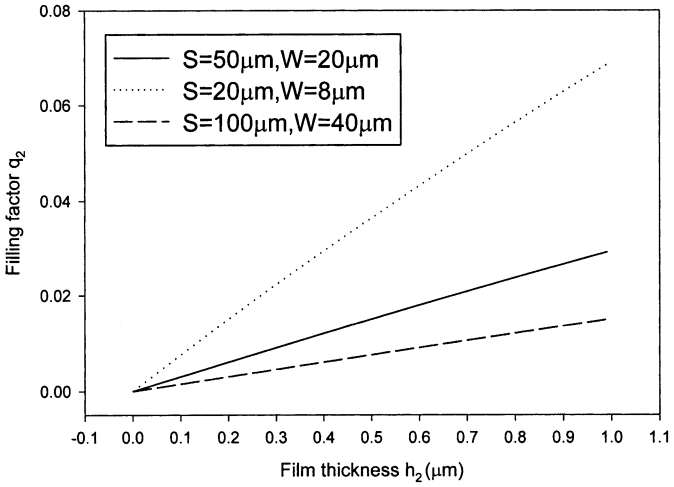

Fig. 8. Calculated filling factors versus BST film thickness for different geometries.

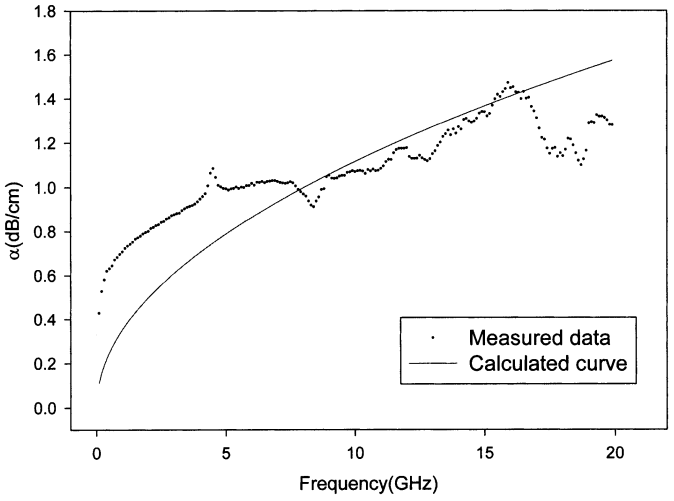

Fig. 9. Comparison of calculated and measured attenuation constant of bare sapphire wafer after TRL calibration.

The surface resistance caused by the normal skin effect is given by

$$R_s = \sqrt{\frac{\omega\mu_0\rho}{2}} \tag{20}$$

where ρ is the resistivity in ohm meters. We can measure the resistivity by the conventional four-point probe method, from which the value $\rho = 6\mu\Omega$ cm can be obtained. The attenuation constant α_c was then calculated by (16)–(20). The calculated result and experimental measured data after TRL calibration are shown in Fig. 9. Although there is some deviation between them, the measured data were still in the expected range of the theoretically calculated result. This reasonable fit between the calculation and experimental measurements of the resistivity can be explained to demonstrate the validity of TRL calibration, because no noticeable loss caused by impedance mismatch exists. The higher attenuation measured at lower frequency (f < 7 GHz) may be due to the finite conductor thickness, where the skin depth is larger than the conductor thickness. In this regime, the surface resistance will be less dependent on the frequency and exhibit a larger attenuation than expected. For $\rho = 6\mu\Omega$ cm, the calculated skin depth is larger than 1 μm at frequencies less than 7 GHz. This can reasonably explain the intersection between experimental and calculated results.

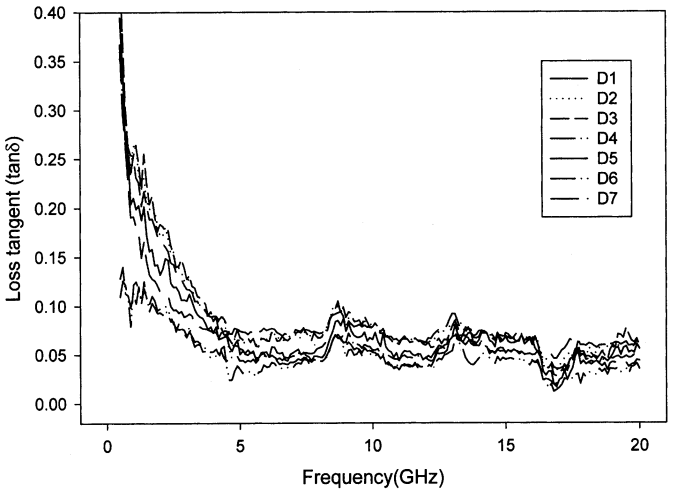

Fig. 10. Calculated loss tangent versus frequency of BST thin films.

For CPW with BST thin films, another important loss is due to the loss tangent of ferroelectric layer. The effective loss tangent is given by

$$\varepsilon_{eff}\tan\delta_{eff} = q_1\varepsilon_{r1}\tan\delta_1 + q_2\varepsilon_{r2}\tan\delta_2. \tag{21}$$

If substrate loss is neglected, the loss tangent of ferroelectric thin film is given by

$$\tan\delta_2 = \frac{\varepsilon_{eff}\tan\delta_{eff}}{q_2\varepsilon_{r2}} \tag{22}$$

where $\tan\delta_{eff}$ is the overall effective loss tangent. $q_1, q_2, \varepsilon_{r2}$, and ε_{eff} were already given in Section VI. The effective loss tangent is calculated by the dielectric attenuation constant [6]:

$$\alpha_d = 0.91\sqrt{\varepsilon_{eff}}f(GHz)\tan\delta_{eff} \quad (dB/cm). \tag{23}$$

The total attenuation is the sum of conductor loss and dielectric loss, and, therefore,

$$\alpha_d = \alpha - \alpha_c. \tag{24}$$

If we assume the conductor loss of the sample is the same as the CPW of a bare sapphire wafer without BST, then, from (2) and (21)–(24), loss tangents are evaluated, as shown in Fig. 10. It is indicated that there is a fast relaxation of loss tangent at low frequency. One possible reason for this phenomenon is the inevitable error of TRL calibration near zero frequency. Further study is needed to clarify this point. A fast relaxation of effective dielectric constant

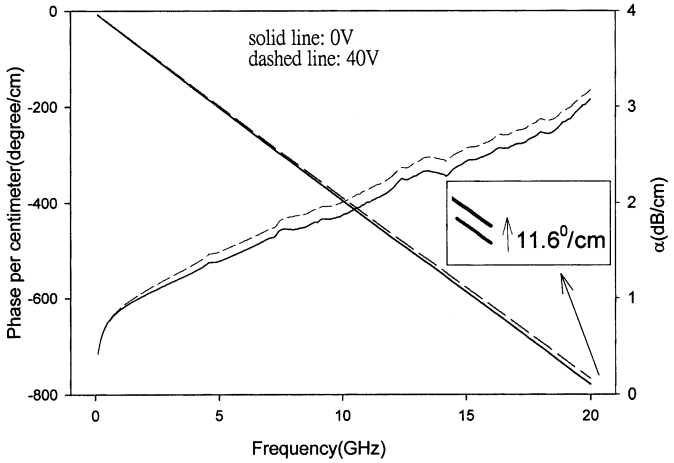

Fig. 11. Phase shift and attenuation constant versus frequency from the sample D7 under bias.

at low frequency (less than 1 GHz) is also observed for each sample and the bare sapphire wafer if (1) is directly applied to extract the effective dielectric constant without subtraction of the offset phase shift $\Delta\phi_0$. However, the dielectric constant of a sapphire wafer is expected to be constant, and, therefore, this offset phase shift was not because of the intrinsic material properties but instead because of the calibration method. Consequently, the offset phase shift should be subtracted to get a more correct effective dielectric constant. The loss tangent curves behave in the same manner with a fast relaxation near zero frequency, and we think this behavior is also caused by the calibration error near zero frequency. However, for the loss tangent, we do not have a straightforward method to subtract the calibration error; therefore, we think the loss tangent value is not reliable at low frequency. At high frequency, the loss tangents are stable and around 0.05, which is reasonable when compared with the capacitance-voltage (C-V) measurement of metal-insulator-metal (MIM) structure.

VIII. Tunability

The tuning behavior of the sample D7 was measured and is shown in Fig. 11. It is indicated that the D7 sample has attenuation less than 3 dB/cm between 100 MHz and 20 GHz and a phase shift of 11.60°/cm at 20 GHz. The attenuation increased slightly when a 40-V bias was applied. The calculated dielectric constant ε_{r2} of BST in D7 under zero bias is 225; at 40-V DC bias, ε_{r2} is 211. Although there is indeed a noticeable change of dielectric constant of the BST thin film, the total tunability is not remarkable. This result is attributed to the small filling factor q_2 (around 1%) of the BST layer. One direct way to enhance the tunability of ferroelectric devices is to improve the intrinsic material property; another way is to enhance the filling factor, which can be achieved by reducing the line width and increasing the film thickness. As shown in Fig. 8, the filling factor significantly increases when the line width is reduced. In addition, reducing the line widths also enhances the electric field and increases the tunability of the material. Therefore, it seems that reducing the line widths is the most effective method for tunable ferroelectric devices to operate at low voltages. However, the attenuation will inevitably increase. Therefore certain trade-offs should be made to achieve the desirable performance of CPW devices.

We can estimate the tunability of the CPW devices with the quasi-TEM analysis as described in Section VI. For example, if S = 20 μm, W = 8 μm, and the thickness of ferroelectric layer is 1 μm, the filling factor q_2 is calculated to be 0.07. If the dielectric constant of the ferroelectric layer changes from 500 to 450 under 40-V DC bias, or equivalently with an electric field of 50 kV/cm as measured by low frequency C-V measurement, then the effective dielectric constant ε_{eff} at zero bias can be estimated to be 39.6; at 40-V bias, ε_{eff} is 36.1. The phase change at 20 GHz is consequently calculated to be 68°/cm. If the attenuation constant is 6 dB/cm, the figure of merit (FOM) of the device is estimated to be 11°/dB. As a result, this method would offer designers a fast tool to estimate the performance of tunable ferroelectric devices.

IX. Conclusions

In this paper, we have developed a detailed and accurate technique to measure the dielectric constant, loss tangent, and tunability of ferroelectric thin films with on-wafer TRL calibration. We have measured the conductor loss and dielectric loss of Al/BST/sapphire CPW transmission lines and found that these losses are not serious. Even at frequencies as high as 20 GHz, the overall attenuation is less than 3 dB/cm. Therefore, if ferroelectric devices can be designed with careful impedance matching, normal metals may be used instead of superconductors. We have also proposed a detailed analysis of tunable CPW transmission lines, which offers a fast tool to estimate the performance of any ferroelectric CPW device before measurement.

Acknowledgment

Dr. Guo-Wei. Huang of the National Nano Device Laboratories is thanked for many useful discussions.

References

[1] D. C. DeGroot, J. A. Beall, R. B. Marks, and D. A. Rudman, "Microwave properties of voltage-tunable $YBa_2Cu_3O_{7-\delta}/SrTiO_3$ coplanar waveguide transmission lines," *IEEE Trans. Appl. Superconduct.*, vol. 5, pp. 2272–2275, 1995.

[2] O. G. Vendik, E. F. Carlsson, P. K. Petrov, R. A. Chakalov, S. S. Gevorgian, and Z. G. Ivanov, "HTS/Ferroelectric CPW structures for voltage tunable phase shifters," in *Proc. 27th Eur. Microwave Conf. Exhibition*, pp. 196–202.

[3] H. D. Wu and F. S. Barnes, "Doped $Ba_{0.6}Sr_{0.4}TiO_3$ thin films for microwave device applications at room temperature," *Integrated Ferroelect.*, vol. 22, pp. 291–305, 1998.
[4] G. Subruamanyam, F. V. Keuls, and F. A. Miranda, "A K-band tunable microstrip bandpass filter using a thin film conductor/ferroelectric/dielectric multiplayer configuration," *IEEE Microwave Guided Wave Lett.*, vol. 8, no. 2, pp. 78–80, Feb. 1998.
[5] D. Galt and J. C. Price, "Ferroelectric thin film characterization using superconducting microstrip resonators," *IEEE Trans. Appl. Superconduct.*, vol. 5, pp. 2575–2578, Jun. 1995.
[6] K. C. Gupta, *Microstrip Lines and Slotlines*. 2nd ed. Boston, MA: Artech House, 1998, ch. 7.
[7] G. F. Engen and C. A. Hoer, "Thru-Reflect-Line: An improved technique for calibrating the dual six-port automatic network analyzer," *IEEE Trans. Microwave Theory Tech.*, vol. MTT-27, no. 12, pp. 987–993, Dec. 1979.
[8] D. Rubin, "De-embedding mm-wave MICs with TRL," *Microwave J.*, pp. 141–150, Jun. 1990.
[9] E. Carlsson and S. Gevorgian, "Conformal mapping of the field and charge distributions in multilayered substrate CPW's," *IEEE Trans. Microwave Theory Tech.*, vol. 47, no. 8, pp. 1544–1552, Aug. 1999.
[10] C. L. Holloway and E. F. Kuester, "A quasi-closed form expression for the conductor loss of CPW lines, with an investigation of edge shape effects," *IEEE Trans. Microwave Theory Tech.*, vol. 43, no. 12, pp. 2695–2701, Dec. 1995.
[11] P. K. Petrov and E. F. Carlsson, "Improved $SrTiO_3$ multilayers for microwave application: Growth and properties," *J. Appl. Phys.*, vol. 84, no. 6, pp. 3134–3140, Sep. 1998.
[12] A. Kozyrev, V. Osadchy, Apavlov, and L. Sengupta, "Application of ferroelectrics in phase shifter design," *IEEE MTT-S Digest*, pp. 1355–1358, 2000.
[13] J. R. Powell, A. Porch, F. Wellhöfer, M. J. Lancaster, T. Bollmeier, and B. Stritzker, "Laser ablated ferroelectric and superconducting thin films for microwave applications," in *IEE Colloquium on Superconducting Microwave Circuits*, pp. 7/1–7/5, 1996.

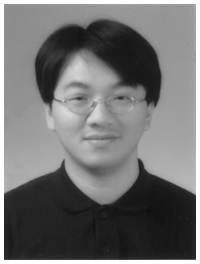

Hang-Ting Lue received the M.S. degree in physics from National Tsing Hua University, Hsinchu, Taiwan, in 1999. He is now pursuing the Ph.D. degree in electrical engineering in National Chiao Tung University, where his current research is focused on the application of ferroelectrics in microwave circuits and micromachined millimeterwave transmission lines and related filters.

Tseung-Yuen Tseng (M'94–SM'94) received the Ph.D. degree in electroceramics from the School of Materials Engineering, Purdue University, West Lafayette, IN, in 1982. Before joining National Chiao-Tung University, Hsinchu, Taiwan R.O.C. in 1983, where he is a now a professor in the Department of Electronics Engineering and the Director of the Institute of Electronics, he was briefly associated with University of Florida. His professional interests are ferroelectric thin films, electronic ceramics, ceramic sensors, and high temperature ceramic superconductors. He has published over 220 research papers.

Dr. Tseng has been elected Fellow of the American Ceramic Society for "his notable contributions to the ceramic arts and sciences." He was the recipient of the Distinguished Research Award of the National Science Council, R.O.C. in 1995–2000, the Ceramic Medal from the Chinese Ceramic Society in 1999, and the Distinguished Electrical Engineering Professor Award from the Chinese Electrical Engineering Society in 2000. He is a registered professional engineer in R.O.C.